

Order, Chaos and Born's Distribution of Bohmian Particles

Athanasios C. Tzemos ^{*,†}  and George Contopoulos [†]

Research Center for Astronomy and Applied Mathematics of the Academy of Athens—Soranou Efessiou 4, GR-11527 Athens, Greece; gcontop@academyofathens.gr

* Correspondence: atzemos@academyofathens.gr

[†] These authors contributed equally to this work.

Abstract: We study order, chaos and ergodicity in the Bohmian trajectories of a 2D quantum harmonic oscillator. We first present all the possible types (chaotic, ordered) of Bohmian trajectories in wavefunctions made of superpositions of two and three energy eigenstates of the oscillator. There is no chaos in the case of two terms and in some cases of three terms. Then, we show the different geometries of nodal points in bipartite Bohmian systems of entangled qubits. Finally, we study multinodal wavefunctions and find that a large number of nodal points does not always imply the dominance of chaos. We show that, in some cases, the Born distribution is dominated by ordered trajectories, something that has a significant impact on the accessibility of Born's rule $P = |\Psi|^2$ by initial distributions of Bohmian particles with $P_0 \neq |\Psi_0|^2$.

Keywords: chaos; Bohmian quantum mechanics; Born's rule

1. Introduction

Bohmian quantum mechanics (BQM) is a trajectory based quantum theory, which predicts the same experimental results [1–7] as standard quantum mechanics. In BQM, the quantum particles evolve according to the so called 'Bohmian equations of motion':

$$M \frac{d\vec{r}}{dt} = \hbar \Im \left(\frac{\nabla \Psi}{\Psi} \right), \quad (1)$$

where $\Psi = |\Psi| \exp(iS/\hbar)$ is the wavefunction, i.e. the solution of the Schrödinger equation

$$-\frac{\hbar^2}{2M} \nabla^2 \Psi + V(x, y) \Psi = i\hbar \frac{\partial \Psi}{\partial t}, \quad (2)$$

Ψ plays the role of a pilot wave which dictates the motion of the quantum particles in space. Thus, BQM is characterised as a pilot wave theory [1,2]. A similar approach was the Madelung hydrodynamic approach [8–10].

The Bohmian equations of motion have some important characteristics:

1. They are deterministic differential equations of first order in time. However, they can be written as second order in time differential equations:

$$\frac{d^2 x}{dt^2} = -\frac{\partial}{\partial x} (V + Q), \quad \frac{d^2 y}{dt^2} = -\frac{\partial}{\partial y} (V + Q), \quad (3)$$

if we introduce

$$Q = -\frac{\hbar^2}{2M} \frac{\nabla^2 |\Psi|}{|\Psi|}, \quad (4)$$

which is the 'Bohmian quantum potential' [11–13] and demand that $\frac{d\vec{r}}{dt}$ is initially given by Equation (1). Q remains the same when $|\Psi|$ is multiplied by a constant, i.e., it



Citation: Tzemos, A.C.; Contopoulos, G. Order, Chaos and Born's Distribution of Bohmian Particles. *Particles* **2023**, *6*, 923–942. <https://doi.org/10.3390/particles6040060>

Academic Editor: Armen Sedrakian

Received: 1 September 2023

Revised: 12 October 2023

Accepted: 25 October 2023

Published: 1 November 2023



Copyright: © 2023 by the authors. Licensee MDPI, Basel, Switzerland. This article is an open access article distributed under the terms and conditions of the Creative Commons Attribution (CC BY) license (<https://creativecommons.org/licenses/by/4.0/>).

does not depend on the magnitude of Ψ . Moreover, it is not externally controlled as the classical potential and includes information for the whole setup of the system. Thus, the Bohmian equations are nonlocal and incorporate, in general, the phenomenon of quantum entanglement in the wavefunction of the system under study. Finally, Q does not go, in general, to zero in the limit $\hbar \rightarrow 0$. Consequently the Bohmian trajectories are different from the classical trajectories.

2. They are highly nonlinear. Thus they allow, in principle, the coexistence of both ordered and chaotic trajectories for any given Bohmian system (chaos refers to the high sensitivity of the trajectories on slight changes in the initial conditions, as in classical mechanics). Consequently, in contrast to the standard quantum mechanics where quantum chaos is not well defined [14,15]), Bohmian quantum mechanics provides us with a natural way to define quantum chaos and study chaotic phenomena in the quantum world by applying all the techniques of the theory of classical dynamical systems [16,17].

Chaos in BQM has attracted the interest of many authors in the past [18–31]. The common conclusion in all these works is that chaos emerges in the close neighbourhood of the nodal points of the wavefunction, i.e., the solutions of the equations $\Psi_{Re} = \Psi_{Im} = 0$ (Ψ is a complex quantity). In general, as a Bohmian particle comes close to a nodal point N , its direction deviates. Due to the non autonomous character of the Bohmian flow the positions of the nodal points are, in general, time-dependent.

In our series of works, we studied in detail the mathematical mechanism behind chaos generation in 2D Bohmian trajectories (for a review up to 2020, see [32] and the references therein). We found the following:

1. In the frame of reference of the moving nodal point ($u = x - x_N, v = y - y_N$), there is a second critical point of the Bohmian flow, the X-point, which is unstable and scatters the incoming Bohmian particles. Every nodal point and its accompanied X-point form a ‘nodal point-X-point complex’ (NPXPC). However, there are also cases where the positions of the nodal points are fixed [31,33].
2. Chaos emerges as the cumulative effect of many close encounters between Bohmian particles and the X-points of the NPXCs. The detection of chaos is usually made by calculating the ‘Lyapunov characteristic number’ (LCN). The finite time LCN is $\chi(t) = \frac{\ln\left(\frac{\xi}{\xi_0}\right)}{t}$, where ξ_0 and ξ are infinitesimal deviations at times $t_0 = 0$ and t correspondingly. Then, $LCN = \lim_{t \rightarrow \infty} \chi(t)$. After many such scattering events, LCN saturates at a positive number, i.e., chaos emerges. On the other hand, when the Bohmian trajectories do not come close to the NPXCs, we have $LCN = 0$, i.e., they are ordered.
3. The geometry of the NPXCs is, in general, time-dependent: the nodal point changes in time from attractor to repeller and vice versa.
4. In multinodal systems, there exist, in general, both moving and fixed nodal points. In these cases, one observes collisions between the moving nodes as well as between the moving and fixed nodes [33].
5. Beside the X-points, there also exist the Y-points, which are unstable points in the inertial frame of reference. Their contribution to chaos is not as strong as that of the X-points, but is not negligible. With the discovery of the Y-points, we practically understand every contribution to the LCN [34].
6. The X-point is always close to the local maximum of the quantum potential in the close neighbourhood of the nodal point [13]. The Y-point does not have a distinguished position on the Q surface [34].
7. There are classically ordered systems whose Bohmian quantum counterparts are chaotic and vice versa.
8. The chaotic Bohmian trajectories are approximately ergodic: the support of the wavefunction consists, in general, of areas of initial conditions whose chaotic trajectories fill the same areas with approximately the same distribution. When the area is the

whole support of Ψ , we have complete ergodicity, and when it is smaller than the support, we have partial ergodicity.

In Figure 1a, we show a typical NPXPC. By fixing the time t to the right hand side of the Bohmian equations and using a new time s for the remaining autonomous system (see [35] for the so called adiabatic approximation), we find two stable (blue) and two unstable (red) asymptotic curves from the X-point. One asymptotic curve forms a spiral around the nodal point N . Trajectories of quantum particles approaching the X-point along paths close to the stable asymptotic curves are deviated along the two unstable directions. This is the main mechanism behind chaos generation. On the other hand, in Figure 1b, we observe the asymptotic curves of a Y-point in a system with two nodal points. The two asymptotic curves spiral around the nodal points N . The Y-points also scatter the approaching trajectories into two opposite directions and contribute to chaos production.

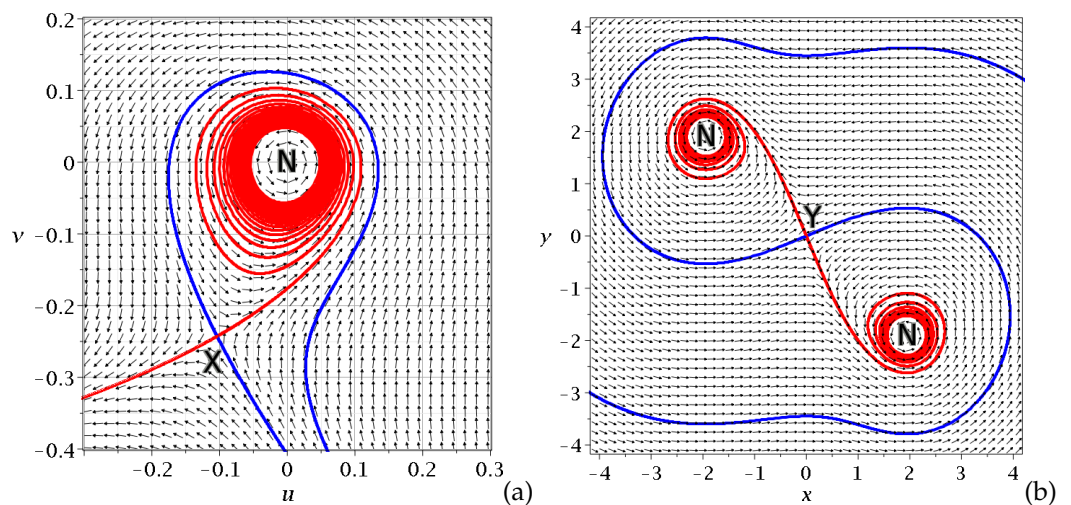


Figure 1. (a) The asymptotic curves of the X-point in the coordinate system of the moving nodal point (u, v) . (b) Asymptotic curves from the Y-point in the inertial system (x, y) .

Most results in Bohmian chaos have been found by studying the quantum harmonic oscillator with incommensurable frequencies. In the 2D case, this system corresponds to the classical potential

$$V = \frac{1}{2}(M_x\omega_x^2x^2 + M_y\omega_y^2y^2). \tag{5}$$

The choice of working with the quantum harmonic oscillator is based on two facts: (a) It is the most well studied quantum system since its wavefunctions are analytically known. (b) Its wavefunctions form a complete basis in Hilbert space, i.e., every quantum state can be written as a linear combination of the energy eigenstates of the quantum harmonic oscillator. Thus, there is no loss of generality.

Despite the many results that have been found in the field of Bohmian Chaos, there are still gaps regarding basic questions in Bohmian Dynamics.

In fact:

1. All the experimental results predicted by the quantum theory are following Born’s rule, according to which the probability density of finding a particle close to a given point of space is $P = |\Psi|^2$ [36]. Bohmian quantum mechanics predicts the same results under the assumption that the Bohmian particles are initially prepared according to Born’s rule (equilibrium states). However, the Bohmian approach allows us, in principle, to consider initial distributions of Bohmian particles where $P_0 \neq |\Psi_0|^2$ [37–44]. Such non equilibrium states can be traced back to the very early times of the Universe, when there were quantum fluctuations during the inflationary period [45–47]. Born’s rule was then supposed to be established later by the action of noise perturbations.

2. As mentioned above, it is well recognised that chaos appears when trajectories approach the nodal points ($\Psi = 0$). Our contribution to this problem has been a study of the necessary conditions for reaching Born’s rule when the initial particle distribution is different ($P_0 \neq |\Psi_0|^2$) without any external perturbation. In general, chaos becomes more evident when the number of the nodal points increases. However, here we show that this is not always true.

In this paper, we study the role of order and chaos in establishing Born’s rule. We emphasize, first, that the Born distribution contains, in general, both ordered and chaotic trajectories. The chaotic trajectories cannot become ordered and vice versa. Therefore, unless we have the correct proportions of chaotic and ordered trajectories we cannot reach the Born distribution [48]. As a consequence, the coexistence of order and chaos in the Bohmian quantum mechanics plays a key role in deriving the same experimental results as those of standard quantum mechanics.

The basic phenomenology of Bohmian trajectories from the standpoint of dynamical systems can be explained with simple wavefunctions of the quantum harmonic oscillator with relatively small number of nodes.

The structure of the present paper is the following: In Section 2, we study linear superpositions of two terms, and then in Section 3, we consider various cases with a third term both with commensurable and incommensurable frequencies. Then, in Section 4, we present the case of entangled Bohmian qubits made of coherent states of the quantum harmonic oscillator and present new results on the dynamics of the nodal points as we construct the Poissonian energy spectrum of the coherent states (this section is accompanied by the Appendix A). In Section 5, we deal with order and chaos in the Born distribution of some multinodal wavefunctions. There, we show that there are cases where a large number of nodes does not guarantee the absence of ordered trajectories. Finally, in Section 6, we draw our conclusions.

2. Superpositions of Two Components

We work, in general, with solutions of the form

$$\Psi = \sum_i c_i \Psi_{m_i, n_i}, \tag{6}$$

where the components of $\Psi_{m,n}(x, y) = \Psi_m(x)\Psi_n(y)$. $\Psi_m(x)$ and $\Psi_n(y)$ are the 1D energy eigenstates the oscillator in x and y coordinates, respectively, i.e.,

$$\Psi_{m,n} = \prod_{q=x}^y N_q \exp\left(-\frac{\omega_q q^2}{2\hbar}\right) \exp\left(-\frac{i}{\hbar} E_s t\right) H_s\left(\sqrt{\frac{M_q \omega_q}{\hbar}} q\right), \tag{7}$$

where $s = m, n$ (integers) for x and y , respectively, and the normalization constant $N_q = \frac{(M_q \omega_q)^{\frac{1}{4}}}{\pi \hbar \sqrt{2^s s!}}$. The functions H_m, H_n are Hermite polynomials in $\sqrt{\frac{M_x \omega_x}{\hbar}} x$ and $\sqrt{\frac{M_y \omega_y}{\hbar}} y$ of degrees m and n , respectively. The energy of the component $\Psi_{m,n}$ is

$$E_{m,n} = E_m + E_n = \left(\frac{1}{2} + m\right) \hbar \omega_x + \left(\frac{1}{2} + n\right) \hbar \omega_y. \tag{8}$$

We consider general solutions of the form (6) with i up to 1, 2, 3 or higher. At the nodal points (x_N, y_N) , we have $\Psi = 0$. In the numerical examples, we set $M_x = M_y = \hbar = \omega_x = 1$ and either an irrational $\omega_y = \sqrt{2}/2$ or a rational ω_y (e.g., $\omega_y = 1$).

The general case of a superposition of two components is

$$\Psi = a \Psi_{m_1, n_1}(x, y) + b \Psi_{m_2, n_2}(x, y), \tag{9}$$

where $a = |a|N_1 \exp(i\phi_1), b = |b|N_2 \exp(i\phi_2)$ with ϕ_1, ϕ_2 are two constant phases. The real and the imaginary parts of Ψ read:

$$\Psi_{Re} = A \cos(E_1t - \phi_1) + B \cos(E_2t - \phi_2) \tag{10}$$

$$\Psi_{Im} = -A \sin(E_1t + \phi_1) - B \sin(E_2t + \phi_2), \tag{11}$$

where

$$A = |a| \exp\left(-\frac{\omega_x x^2 + \omega_y y^2}{2}\right) H_{m_1} H_{n_1}, \quad B = |b| \exp\left(-\frac{\omega_x x^2 + \omega_y y^2}{2}\right) H_{m_2} H_{n_2}. \tag{12}$$

If $AB \neq 0$, then the nodal points appear when

$$\frac{-A}{B} = \frac{\cos(E_2t - \phi_2)}{\cos(E_1t - \phi_1)} = \frac{\sin(E_2t - \phi_2)}{\sin(E_1t - \phi_1)}. \tag{13}$$

In this case the nodes exist only at times when

$$\sin[(E_1 - E_2)t - (\phi_1 - \phi_2)] = 0. \tag{14}$$

Therefore, in general, there are no such nodal points. On the other hand, we have non moving nodal points if $A = B = 0$, which are the solutions of the equation

$$H_{m_1}(\sqrt{\omega_x}x)H_{n_1}(\sqrt{\omega_y}y) = H_{m_2}(\sqrt{\omega_x}x)H_{n_2}(\sqrt{\omega_y}y) = 0. \tag{15}$$

This implies that the x -component of the nodal point is a root of $H_{m_1}(\sqrt{\omega_x}x_N) = 0$ or of $H_{m_2}(\sqrt{\omega_x}x_N) = 0$. In the first case, we must have $H_{n_2}(\sqrt{\omega_y}y_N) = 0$, while in the second case, we must have $H_{n_1}(\sqrt{\omega_y}y_N) = 0$. For the wavefunction $\Psi = a\Psi_{1,2} + b\Psi_{2,1}$ with $\omega_x = 1, \omega_y = \sqrt{2}/2$, we have the roots of $H_1(\sqrt{\omega_x}x_N) = 0, H_2(\sqrt{\omega_y}y_N) = 0$ and $H_2(\sqrt{\omega_x}x_N) = 0, H_1(\sqrt{\omega_y}y_N) = 0$. Since the Hermitian polynomials have real roots, the total number of nodes is equal to $(m_1n_2 + m_2n_1)$. Thus, in the case $\Psi = a\Psi_{1,2} + b\Psi_{2,1}$ with $\omega_x = 1, \omega_y = \sqrt{2}/2$, we have five nodal points (Figure 2a): $(0, 0), (\pm\sqrt{2}/2, \pm 2^{-1/4})$.

The Bohmian equations of motion are

$$\frac{dx}{dt} = \frac{1}{G} \left(\left(\frac{\partial A}{\partial x} B - \frac{\partial B}{\partial x} A \right) \sin[(E_1 - E_2)t - (\phi_1 - \phi_2)] \right) \tag{16}$$

$$\frac{dy}{dt} = \frac{1}{G} \left(\left(\frac{\partial A}{\partial y} B - \frac{\partial B}{\partial y} A \right) \sin[(E_1 - E_2)t - (\phi_1 - \phi_2)] \right), \tag{17}$$

with

$$G = A^2 + B^2 + 2AB \cos[(E_1 - E_2)t - (\phi_1 - \phi_2)]. \tag{18}$$

From Equations (16) and (17), we derive

$$\frac{dy}{dx} = \frac{\frac{\partial A}{\partial y} B - \frac{\partial B}{\partial y} A}{\frac{\partial A}{\partial x} B - \frac{\partial B}{\partial x} A}. \tag{19}$$

This equation is time-independent and thus it gives y as a function of x , i.e., it represents a curve on the inertial $x - y$ plane. Furthermore, the Equations (16) and (17) give $dx/dt = 0, dy/dt = 0$ when $\theta = (E_1 - E_2)t - (\phi_1 - \phi_2) = 0, \pi, 2\pi, \text{etc.}$, i.e., a particle has zero velocity at the initial point $\theta = 0$ and at the final point $\theta = \pi$. After $\theta = \pi$, it retraces the trajectory in the opposite way and comes back to the original point at $\theta = 2\pi$. Thus, the motions are periodic with period $T = 2\pi/(E_1 - E_2)$. This is equal to $T = 21.452$ when $\omega_x = 1, \omega_y = \sqrt{2}/2, m_1 = 1, n_1 = 2, m_2 = 2, n_2 = 1$.

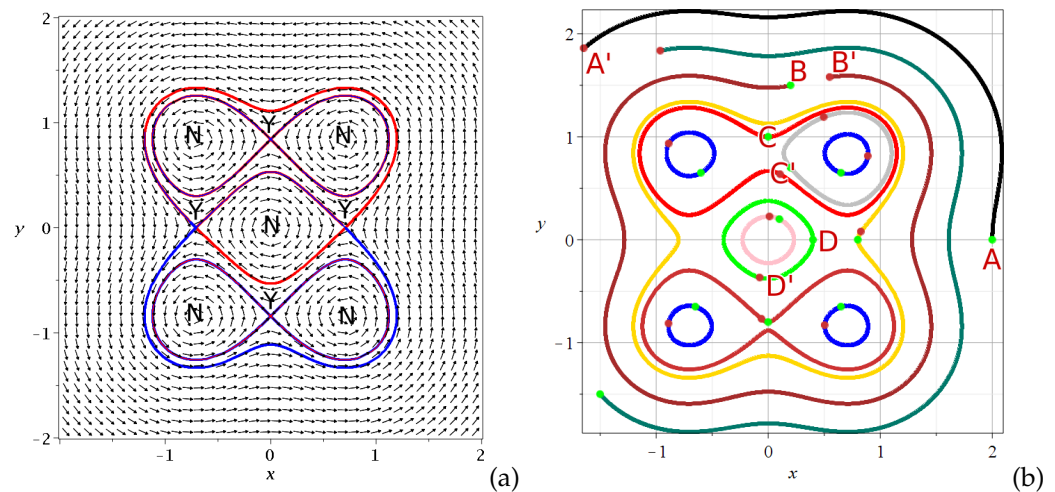


Figure 2. The case of $\Psi = a\Psi_{1,2} + b\Psi_{2,1}$ with $a = 1, b = \sqrt{2}$: (a) The flow on the inertial plane (x, y) , the nodal points and the Y-points with their asymptotic curves (b) Some periodic trajectories. The green dots refer to the initial conditions and the red dots refer to the time $T/2$.

The fact that the trajectories are periodic does not depend on the values of $\omega_x, \omega_y, \phi_1, \phi_2$. Thus, it is also true when $\phi_1 = \phi_2 = 0$, i.e., when a and b are real. For example, in Figure 2a, we show the Bohmian flow when $a = 1, b = \sqrt{2}, \omega_x = 1, \omega_y = \sqrt{2}/2$. Besides the five nodal points, there are also four Y-points. These are found by setting the Bohmian velocities (16) and (17) equal to zero. Thus, the Y-points are at $(0, \pm 2^{-1/4})$ and $(\pm \frac{\sqrt{2}}{2}, 0)$. The asymptotic curves from the upper and lower Y-points for $t = 0$ have the shape of ∞ . The stable and unstable asymptotic curves coincide and there are no homoclinic intersections. This form is consistent with the fact that no chaos appears in this case. The left and right Y-points also generate two stable and two unstable coinciding asymptotic curves, but these curves join two Y-points. The nodal points satisfy the equations

$$a\Psi_{m_1, n_1} \frac{\cos(E_1 t - \phi_1)}{\sin(E_1 t - \phi_1)} + b\Psi_{m_2, n_2} \frac{\cos(E_2 t - \phi_2)}{\sin(E_2 t - \phi_2)} = 0. \tag{20}$$

Therefore, the nodal points are fixed and do not move.

Some trajectories are shown in Figure 2b. The outermost trajectory AA' (black) starts at $A(2, 0)$, reaches a point A' at a time $T/2$ and returns along the same path to A after time T . Similar results are found for larger values of m and n if the differences in the m 's and the n 's in the three terms are equal to 2 and in some more general cases. But in any case, all these cases are exceptional (see Section 6).

The second trajectory (brown) starts at $B(0.2, 1.5)$ and makes almost a complete turn moving counterclockwise. It reaches the final point B' after a time $T/2$ and returns along the same path to the original point B .

The third trajectory (red) starts at $C(0, 1)$ counterclockwise. It makes first a complete turn and it comes again close to C (a little below it). Then, it makes a little more than half of a rotation, a little inside the original points of the curve, reaches the final point C' , and then returns along the same path.

The fourth trajectory (green) starts at $D(0.65, 0.65)$ and makes about seven rotations clockwise, each time slightly inside the previous one. It terminates at a point D' and then it returns to D along the same path.

All the trajectories have the same period, but those starting close to the nodal point make several rotations around the nodal point before reaching the final point.

In other cases of $\Psi = a\Psi_{m_1, n_1} + b\Psi_{m_2, n_2}$, we may have many nodal points, e.g., in the case $\Psi = a\Psi_{4,5} + b\Psi_{5,7}$, we have 59 nodal points and many Y-points between them (Figure 3). But the asymptotic curves coincide and do not intersect at homoclinic or

heteroclinic points. The trajectories are all periodic, although in some cases, they look very complicated.

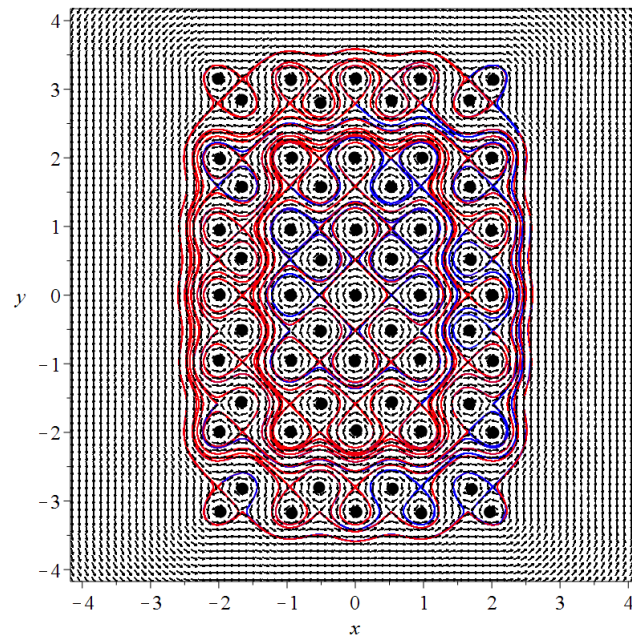


Figure 3. The Bohmian flow with the nodal points and the Y-points along with their asymptotic curves of the wavefunction $\Psi = a\Psi_{5,6} + b\Psi_{4,7}$ with $a = 1, b = \sqrt{2}$. Both nodal points and Y-points do not move. All trajectories are ordered in this case.

This last example is surprising because in this case, there are many nodal points, and one may expect that trajectories starting close to any one of them should be chaotic. But no periodic orbit can come arbitrarily close to any nodal point.

As a conclusion, in the case of two components of the wavefunction, all the trajectories are ordered (periodic) and there is no chaos, although the system of Equation (9) is entangled. A particular subcase is when $a \neq 0, b = 0$, i.e., if we have only one component, where again there is no chaos.

3. Superpositions of Three Components

The superpositions of the form

$$\Psi = a\Psi_{m_1,n_1} + b\Psi_{m_2,n_2} + c\Psi_{m_3,n_3} \tag{21}$$

have been studied extensively up to now [25,28,34,35], since they are the simplest choice for the observation of chaos, as already pointed out in [25].

3.1. Incommensurable Frequencies

Most significant results in the study of Bohmian chaos have been found by using (21) with irrational frequencies [30]. In the general case of (21), the values of Ψ_{Re} and Ψ_{Im} read

$$\begin{aligned} \Psi_{Re} &= \pm A \cos \left[\left(m_1\omega_x + n_1\omega_y + \frac{\omega_x + \omega_y}{2} \right) t \right] \pm B \cos \left[\left(m_2\omega_x + n_2\omega_y + \frac{\omega_x + \omega_y}{2} \right) t \right] \\ \Psi_{Im} &\pm C \cos \left[\left(m_3\omega_x + n_3\omega_y + \frac{\omega_x + \omega_y}{2} \right) t \right], \end{aligned} \tag{22}$$

where A, B are as in (12) and $C = |c|N_3 \exp(-\frac{\omega_x x^2 + \omega_y y^2}{2})H_{m_3}H_{n_3}$. The corresponding Bohmian equations of motion are

$$\begin{aligned} \frac{dx}{dt} = \frac{1}{G} & \left(\left(A \frac{\partial B}{\partial x} - B \frac{\partial A}{\partial x} \right) \sin[(m_1 - m_2)\omega_1 t + (n_1 - n_2)\omega_2 t] \right. \\ & + \left(A \frac{\partial C}{\partial x} - C \frac{\partial A}{\partial x} \right) \sin[(m_1 - m_3)\omega_1 t + (n_1 - n_3)\omega_2 t] \\ & \left. + \left(B \frac{\partial C}{\partial x} - C \frac{\partial B}{\partial x} \right) \sin[(m_2 - m_3)\omega_1 t + (n_2 - n_3)\omega_2 t] \right), \end{aligned} \tag{23}$$

where

$$\begin{aligned} G = & A^2 + B^2 + C^2 + 2AB \cos[(m_1 - m_2)\omega_x t + (n_1 - n_2)\omega_y t] \\ & + 2AC \cos[(m_1 - m_3)\omega_x t + (n_1 - n_3)\omega_y t] \\ & + 2BC \cos[(m_2 - m_3)\omega_x t + (n_2 - n_3)\omega_y t]. \end{aligned} \tag{24}$$

The form of $\frac{dy}{dt}$ is similar with replacement of x with y . Similar equations are found if we have more than three terms of the form (7). Then, we have extra terms in dx/dt and dy/dt with sines of the form $\sin[(m_i - m_j)\omega_x t + (n_i - n_j)\omega_y t]$ in the numerator and $\cos[(m_i - m_j)\omega_x t + (n_i - n_j)\omega_y t]$ in the denominator G .

In general, the systems with three components has both chaos and order. However, there are exceptional cases without chaos. A particular case is when $m_1 = 0, n_1 = 1, m_2 = 2, n_2 = 3, m_3 = 4, n_3 = 5$. Then, since the Hermite polynomials in y are of odd order, y is a common factor in the defining equations of the nodal points, i.e.,

$$\begin{aligned} \frac{\Psi_{Re}}{\Psi_{Im}} = & Lye^{-\frac{\omega_1 x^2 - \omega_y y^2}{2}} \left(\frac{2\sqrt{5}c}{15} (\omega_2^2 y^4 - 5\omega_2 y^2 + \frac{15}{4}) (\omega_1^2 x^4 - 3\omega_1 x^2 + \frac{3}{4}) \cos\left(-\frac{t(9\omega_1 + 11\omega_2)}{2}\right) \right. \\ & \left. + \frac{2b\sqrt{3}}{3} (\omega_1 x^2 - \frac{1}{2}) (\omega_2^2 - \frac{3}{2}) \cos\left(\frac{t(5\omega_1 + 7\omega_2)}{2}\right) + a \frac{\cos\left(-\frac{t(\omega_1 + 3\omega_2)}{2}\right)}{\sin\left(-\frac{t(\omega_1 + 3\omega_2)}{2}\right)} \right), \end{aligned} \tag{25}$$

with $L = \frac{\sqrt{2}}{\sqrt{\pi}} \omega_1^{\frac{1}{4}} \omega_2^{\frac{3}{4}}$. Thus, we find that Ψ vanishes on the x -axis, and it has no isolated nodal points. Moreover, in the right hand side of the corresponding Bohmian equations, there are trigonometric terms of only one angle, $2t(\omega_x + \omega_y)$, i.e., the vector flow has a period $T = \pi/(\omega_x + \omega_y)$, and since at $t = 0$, both components of the Bohmian velocity are equal to zero, all Bohmian trajectories are periodic. In Figure 4a, we plot the Bohmian flow at $t = 0.02$ along with the invariant curves of the Y -points. There are eight Y -points ($Y_1 \dots Y_8$). We observe the complete symmetry of the arrows with respect to the x -axis. The unstable invariant curves from the Y -points (red color) go to infinity along the directions of the x and y axes, while the stable curves (blue color) are of finite length. In fact, they terminate at a repelling fixed point of the frozen flow, e.g., the stable asymptotic curves that seem to join Y_1 with Y_3 in fact terminate close to a point between Y_1 and Y_3 (green dot). The flow changes in time, but the nodal points and the Y -points do not change. The trajectories in this case are periodic, e.g., the trajectory of Figure 4b starts at A , reaches the final point A' , and then returns to A along the same path.

Similar results are found for larger values of m and n if the differences in the m 's and the n 's are equal. However, all these cases are exceptional.

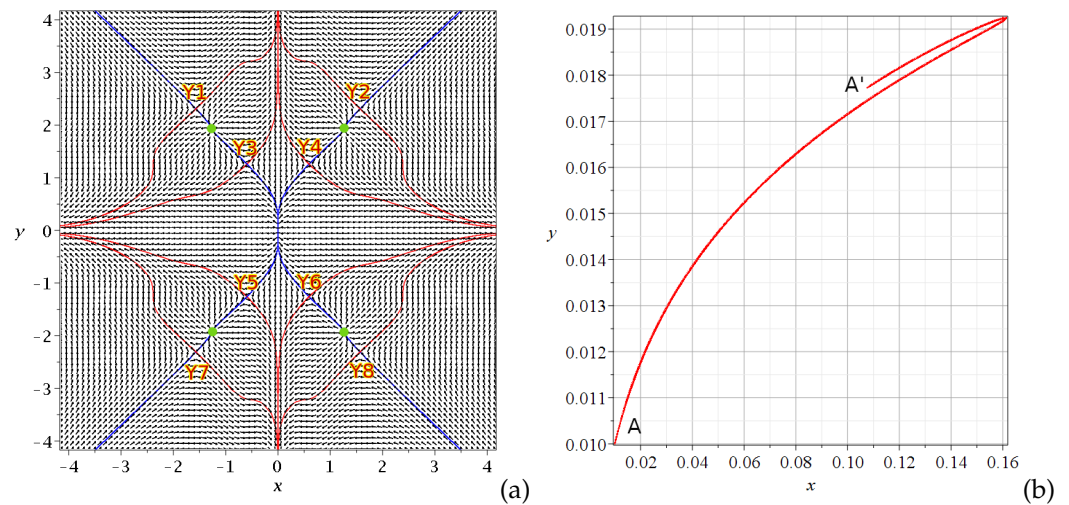


Figure 4. (a) The Bohmian flow at $t = 0.02$ in the case $\Psi = a\Psi_{0,1} + b\Psi_{2,3} + c\Psi_{4,5}$ and the invariant curves of the Y-points. (b) A periodic trajectory with $x(0) = y(0) = 0.01$ ($\omega_x = 1, \omega_y = \sqrt{2}/2, a = 1, b = \sqrt{2}, c = \sqrt{2}/2$).

3.2. Commensurable Frequencies

If, in a system of three components, $\Psi = a\Psi_{m_1, n_1} + b\Psi_{m_2, n_2} + c\Psi_{m_3, n_3}$ the ratio ω_x/ω_y is rational, we have $\omega_x = N_1\omega$ and $\omega_y = N_2\omega$, where N_1/N_2 is an irreducible fraction. The corresponding Bohmian equations then have factors $\sin(N\omega t)$ in the numerator and $\cos(N\omega t)$ in the denominator. Therefore, the numerators have the factor $\sin(\omega t)$ and they become zero at $t = k\pi/\omega$ ($k = 0, 1, 2, \dots$) and, by following the arguments of Section 2, we find that all Bohmian trajectories are periodic.

For example, in the case $m_1 = n_1 = 0, m_2 = 1, n_2 = 0, m_3 = 0, n_3 = 1$ with $\omega_x = \omega_y = 1$, we obtain

$$\Psi_{Re} = \frac{1}{\sqrt{\pi}} \exp\left(-\frac{x^2 + y^2}{2}\right) \left(a \cos(t) + (bx + cy)\sqrt{2} \cos(2t)\right) \tag{26}$$

$$\Psi_{Im} = -\frac{1}{\sqrt{\pi}} \exp\left(-\frac{x^2 + y^2}{2}\right) \left(a \sin(t) + (bx + cy)\sqrt{2} \sin(2t)\right). \tag{27}$$

The nodal points should have

$$a \cos(t) + (bx + cy)\sqrt{2}(2 \cos^2(t) - 1) = 0 \tag{28}$$

$$\sin(t)[(a + 2\sqrt{2}(bx + cy) \cos(t))] = 0. \tag{29}$$

But these equations cannot be satisfied unless $\sin(t) = 0$. Thus, in general, there are no nodal points.

The corresponding Bohmian equations read

$$\frac{dx}{dt} = -\frac{ab\sqrt{2} \sin(t)}{G'}, \quad \frac{dy}{dt} = -\frac{ac\sqrt{2} \sin(t)}{G'}, \tag{30}$$

with

$$G' = [a^2 + 2(bx + cy)^2 + 2a\sqrt{2}(bx + cy) \cos(t)]. \tag{31}$$

As a consequence, $dy/dx = c/b$, i.e., $y = \frac{c}{b}x + C$. The solutions of the Bohmian equation (30) are of the form $x = f_x(\cos(t)), y = f_y(\cos(t))$.

Therefore, the stroboscopic points coincide at the times when $\cos(t) = 1$, e.g., in the case $b = c = \sqrt{2\pi}/2$ we have taken 17 points along the $y = x$ axis and the stroboscopic points of every trajectory are fixed (Figure 5a). If, however, the factors b, c are complex,

i.e., $b = |b| \exp(i\gamma_1), c = |c| \exp(i\gamma_2)$ with $\gamma_1 \neq \gamma_2$, then the stroboscopic images of the 17 points along the $y = x$ axis give both order and chaos (Figure 5b).

In order to find how Figure 5a is transformed into Figure 5b, we have taken in the values of b, c the same γ_1, γ_2 but multiplied them by a factor of ϵ ranging from $\epsilon = 0$ (Figure 5a) up to $\epsilon = 1$ (Figure 5a–f). The stroboscopic images are taken up to a time $t = 1000\pi$. In Figure 5c, we have taken $\epsilon = 0.8$. This figure contains both ordered and chaotic stroboscopic images, but displaced with respect to Figure 5b.

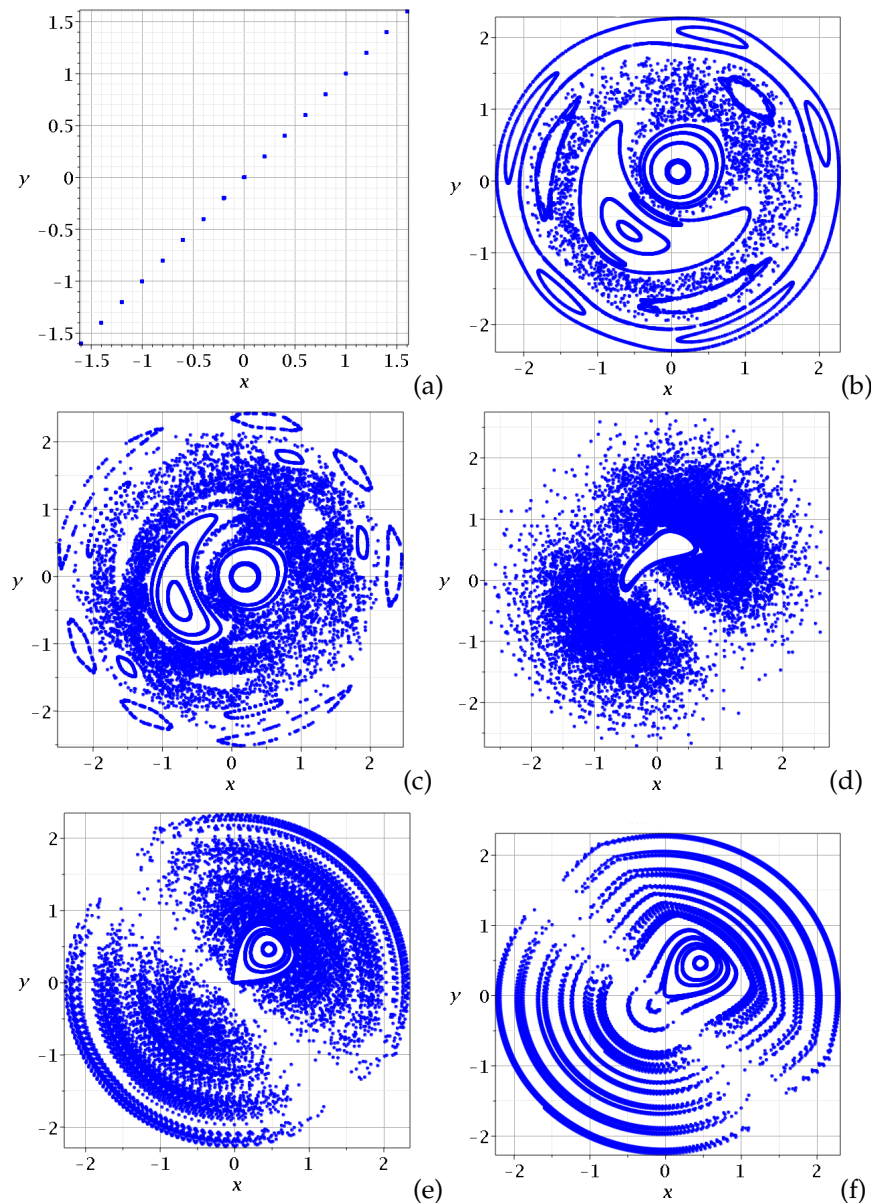


Figure 5. Stroboscopic images in the case of complex weights in Ψ with $a = 0.17651\sqrt{\pi}, b = c = \sqrt{2\pi}/2$, and $\gamma_1 = 3.876968\epsilon, \gamma_2 = 2.684916\epsilon$ (see [28]) for different values of ϵ : (a) $\epsilon = 0$, (b) $\epsilon = 1$, (c) $\epsilon = 0.8$, (d) $\epsilon = 0.3$, (e) $\epsilon = 0.04$, (f) $\epsilon = 0.01$.

In Figure 5d ($\epsilon = 0.3$), the main island of stability is smaller in size and in Figure 5e ($\epsilon = 0.04$), it takes a position along the diagonal $x = y$. Finally, in Figure 5f ($\epsilon = 0.01$), the invariant curves fill most of the space (x, y) symmetrically with respect to the axis $x = y$, and the chaotic regions are very small. Therefore, if ϵ is slightly different from zero, then the fixed points of Figure 5a change into a set of large ordered curves, with only a little chaos between them. As ϵ increases, the chaotic regions increase, but some ordered trajectories remain.

In Figure 6, we see three ordered trajectories (red) and the corresponding stroboscopic invariant curves (black), while in Figure 6d, we see a chaotic trajectory whose stroboscopic images are scattered. All these figures refer to the case of Figure 5b.

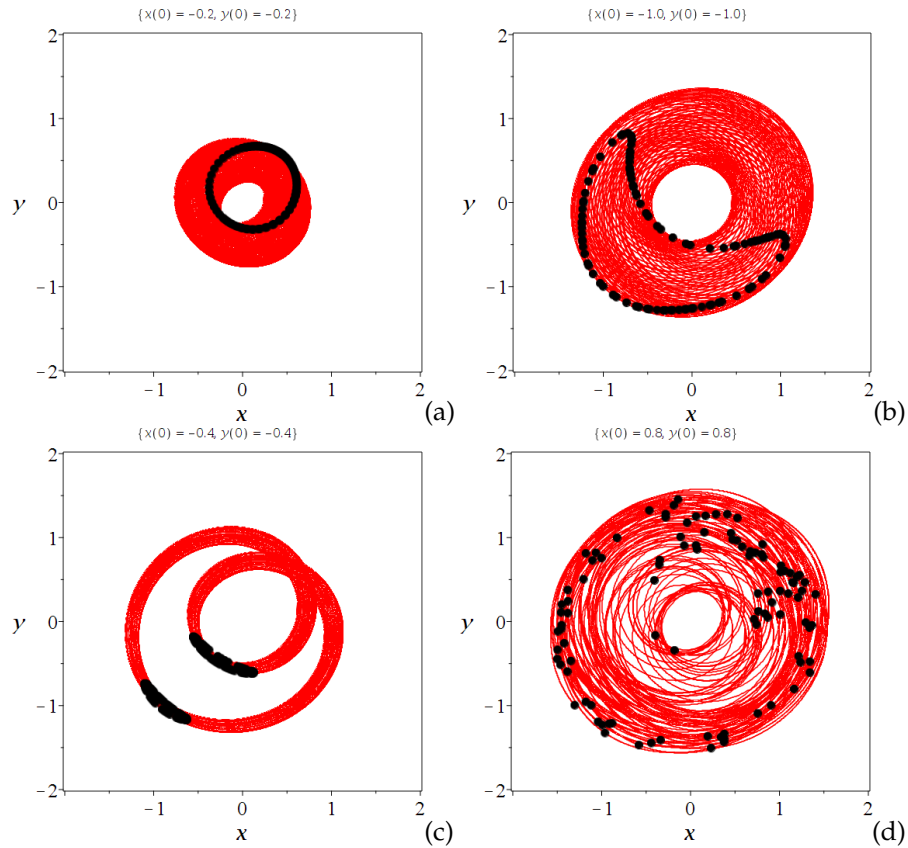


Figure 6. (a–c): Three ordered trajectories (red) and the corresponding stroboscopic invariant curves (see Figure 5b). (d) A chaotic trajectory (red). In this case, the stroboscopic images of the initial point are randomly scattered. ($a = 0.17651\sqrt{\pi}$, $b = c = \sqrt{2\pi}/2$, and $\gamma_1 = 3.876968$, $\gamma_2 = 2.684916$).

The coexistence of ordered and chaotic trajectories in the support of the wavefunction (the region where $|\Psi|^2$ is not negligible) affects the accessibility of the Born rule distribution. Namely, the existence of the islands of stability implies that all trajectories inside them will never escape to other regions of space. In fact, it is possible to define an approximate integral of motion $S(x, y) = K$ inside the islands of stability and interpret the observed asymptotic curves as the level curves of S for various values of K . Thus, when we have islands of stability, any initial distribution with $P_0 \neq |\Psi_0|^2$ will never approach $P = |\Psi|^2$.

4. Bohmian Qubits

While the possible combinations of quantum numbers and the number of terms in a wavefunction describing a quantum oscillator are infinitely many (due to the linearity of Schrödinger’s equation), most basic orbital characteristics of the corresponding Bohmian trajectories can be studied with systems with few nodal points and a small number of terms. However, of special importance is the case of coherent states of the harmonic oscillator, which was our choice in a series of previous papers of ours that dealt with the relation between order, chaos and entanglement [49] in bipartite Bohmian qubit systems [48,50] (for entanglement in BQM, see also [51–53]).

A coherent state of a quantum harmonic oscillator corresponding to the classical system

$$H = \frac{1}{2}M_x\omega_x^2x^2 + \frac{p^2}{2M_x}, \tag{32}$$

is defined as the eigenstate of the annihilation operator \hat{a} :

$$\hat{a}|\alpha\rangle = A|\alpha\rangle. \tag{33}$$

The eigenvalue $A = |A| \exp(i\theta)$ is complex because the operator \hat{a} is not hermitian. Furthermore, $|A|$ is the amplitude and θ the phase of the state $|\alpha\rangle$. A coherent state reads

$$|\alpha\rangle = e^{-\frac{1}{2}|A|^2} \sum_{n=0}^{\infty} \frac{A^n}{\sqrt{n!}} |n\rangle, \tag{34}$$

where $|n\rangle$ are the eigenvectors of the Hamiltonian operator $\hat{H} = \hbar\omega_q(\hat{a}_q^\dagger \hat{a}_q + \frac{1}{2})$ with $q = x, y$. The discrete energy spectrum of a coherent state follows Poissonian statistics (Figure 7) [54], i.e., the probability of detecting the energy level n in the state $|\alpha\rangle$ is

$$P(n) = |\langle n|\alpha\rangle|^2 = \frac{e^{-\langle n\rangle} \langle n\rangle^n}{n!}. \tag{35}$$

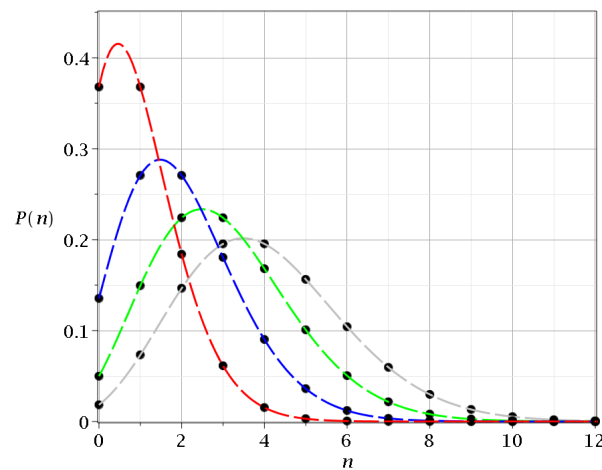


Figure 7. The Poissonian distribution of energy levels in a coherent state for $\langle n \rangle = 1$ (red curve) $\langle n \rangle = 2$ (blue curve), $\langle n \rangle = 3$ (green curve) and $\langle n \rangle = 4$ (grey curve).

From the general theory of random distributions, we know that the mean value $\langle n \rangle$ and the variance $(\Delta n)^2$ are both constant, equal to $|A|^2$, and $\sum_{n=0}^{\infty} P(n) = 1$. The time-dependent wavefunction of a 1D coherent state in the position representation reads:

$$Y(x, t) = e^{-\frac{1}{2}a_0^2} e^{\frac{-i\omega_x t}{2}} \sum_{n=0}^{n_f} \frac{(a_0 e^{i\sigma_x} e^{-i\omega_x t})^n}{\sqrt{n!}} \psi_n(x), \tag{36}$$

where

$$\psi_n(x) = \frac{1}{\sqrt{2^n n!}} \left(\frac{M_x \omega_x}{\pi \hbar} \right)^{\frac{1}{4}} e^{-\frac{M_x \omega_x x^2}{2\hbar}} H_n \left(\sqrt{\frac{M_x \omega_x}{\hbar}} x \right), n = 0, 1, 2, \dots, \tag{37}$$

and $H_n(q) = (-1)^n e^{q^2} \frac{d^n}{dq^n} (e^{-q^2})$ are the corresponding Hermite polynomials. In a full coherent state, we have $n_f = \infty$, while $a_0 = |A(0)|, \sigma_x, \omega_x, M_x$ are the initial values of the amplitude, the phase, the frequency and the mass of the oscillator (and similarly for the corresponding parameters in the y direction). In our calculations, we take $M_x = M_y = \hbar = 1$.

In our previous works [48], we studied in detail both cases of ideal and non-ideal qubits from the perspective of entanglement, ergodicity, and Born’s rule. However, it is interesting to see how the Bohmian flow changes by adding increasing amounts of energy terms by increasing the number n_f in the coherent states in a wavefunction of the form

$$Y = c_1 Y_R(x, t) Y_L(y, t) + c_2 Y_L(x, t) Y_R(y, t), \tag{38}$$

where

$$Y_R(x, t) = Y(x, t; \sigma_x = 0), Y_L(x, t) = Y(x, t; \sigma_x = \pi) \tag{39}$$

and similarly for the coordinate y . In the limit of infinite number of energies and with a_0 sufficiently large we showed that Y_R, Y_L define the basis states of a qubit (see [48,55,56]).

As the functions Y_R, Y_L are sums of terms $\Psi_0, \Psi_1, \Psi_2, \dots$ of order (degree in x and y) $0, 1, 2, \dots$ with coefficients as in Equations (36) and (37), the total function Ψ is a superposition of terms $\Psi_{m,n}$ as in Equation (7) with appropriate coefficients. As regards the number of the necessary terms for the production of chaos, there is an ambiguity. If Ψ is a sum of terms of the form

$$\Psi = \sum_{i=1}^{i_{max}} c_i \Psi_i, \tag{40}$$

with $\Psi_i = \Psi_{m_i} \Psi_{n_i}$, then in order to observe chaos, we need to have $i_{max} \geq 3$ (Sections 2 and 3), as it was already shown by Parmenter and Valentine in [18]. On the other hand, if the partial functions are not of the form $\Psi_{m_i} \Psi_{n_i}$, we observe chaos even if $i_{max} = 2$, e.g., in the particular case of qubits $\Psi = c_1 Y_R Y_L + c_2 Y_L Y_R$ (Equation (38)), we have two basic states, and for $c_1 c_2 \neq 0$, there is coexistence of order and chaos. Whenever c_1 or c_2 is zero, we have no entanglement (product state), and the Bohmian system is decoupled; thus, we observe only ordered trajectories. On the other hand, if we truncate Y_R, Y_L at an order n_f and express them in terms of the form $\Psi_{m_i} \Psi_{n_i}$ as in Equation (40), we find $(n_f + 1)^2$ terms (because zero order terms are also counted). Thus, even if $n_f = 1$, there are four terms of the form $\Psi_{0,0}, \Psi_{0,1}, \Psi_{1,0}, \Psi_{1,1}$ (see Appendix A). Therefore, in this case, there is chaos (except if $c_1 c_2 = 0$) because we have four terms of the form (40), although we have two terms of the form (38).

A similar situation appears in the examples of Makowski [25,26], which are similar to our wavefunctions with two terms given by Equation (9). However, we take constant phases ϕ_1 and ϕ_2 , while in Makowski's works, the phases depend on x and y . In such cases, two terms are sufficient for chaos generation, but when ϕ_1, ϕ_2 are constant, all Bohmian trajectories are ordered (Section 2).

In Figure 8, we observe the Bohmian flow at $t = 0.53$ for various truncations of the energies in the coherent states (but the same for both x and y coordinates) in the region $x, y \in [-3, 3]$. When the truncation order is $n_f = 12$, we find 30 nodal points (Figure 8a), and for $n_f = 20$ (Figure 8b), we find 50 nodal points (but there are further points at larger distances outside this square). We see that, as n increases, most nodal points tend to move away from the central area and become aligned along the straight line $x = y$ when $n \rightarrow \infty$ (see Figure 8c). This is exactly the line of the infinitely many nodal points of the full qubit case (Figure 8d).

A remarkable fact is that, while in the case of the truncated wavefunctions, the analytical calculation of the positions of the nodal points is practically tedious, when $n_f > 1$, as we increase the truncation order, in the full qubit case, we managed to analytically calculate the positions of the infinitely many nodes. The simplicity of the form of the probability density $P = |\Psi|^2$, which is characterised by two well defined blobs that collide from time to time, was very useful for us in order to understand chaos generation both from the dynamics of the nodes and the dynamics of P (see [48]).

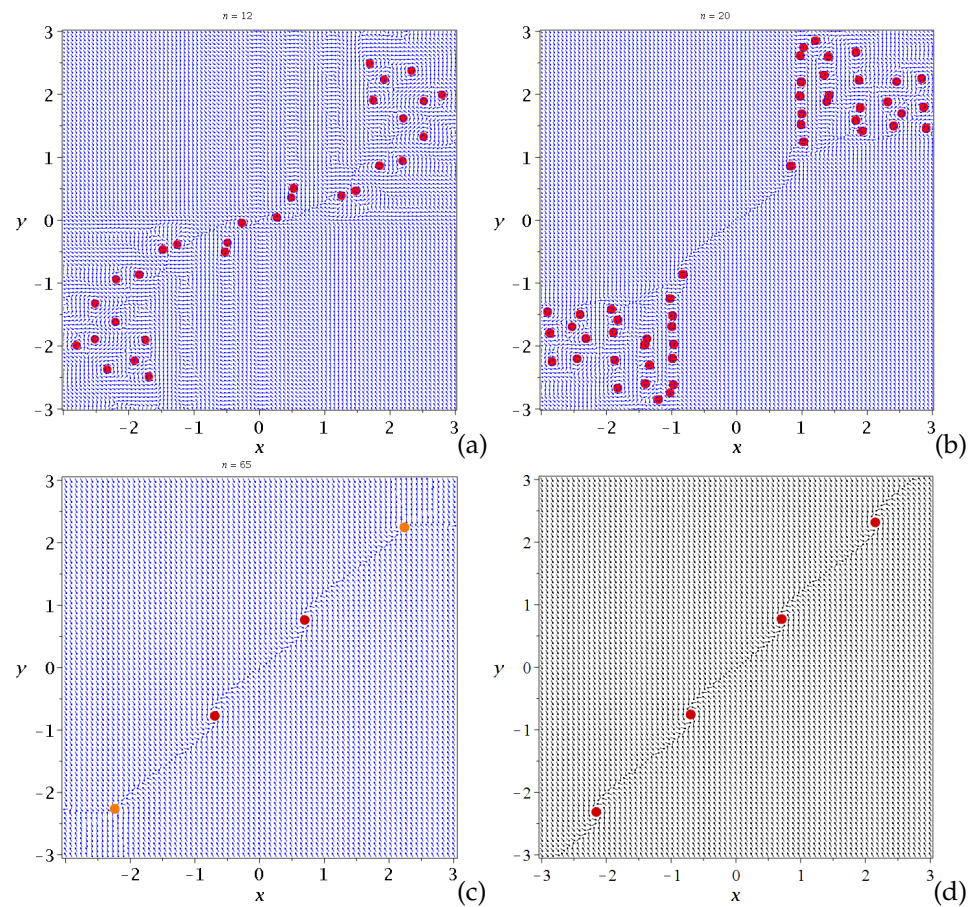


Figure 8. The Bohmian flow at $t = 0.53$ and for various truncations of the energies inside the coherent states of maximally entangled qubits ($\omega_x = 1, \omega_y = \sqrt{3}$): (a) $n = 12$, (b) $n = 20$, (c) $n = 65$. We observe the gradual change in the positions of the nodal points on the $x - y$ plane. We observe how at the truncation $n = 65$ the nodal points tend to align on a straight line, i.e., to reach the geometry of full qubits, which is that of (d). The two central nodal points of (c) perfectly match those of (d), while the outer ones (orange dots) are very close. We work with a common amplitude $a_0 = 2.5$ in both x and y directions.

5. Ergodicity and Born’s Rule

It is widely believed that if the number of nodal points increases, we have more chaotic trajectories, and Born’s rule is established after a long time from more initial distributions.

However, we have seen in Section 3 that there are some cases where no chaos appears at all, even when the number of nodal points is large. Nevertheless, these cases are exceptional, and in most systems with three or more components, we find many chaotic trajectories.

The chaotic trajectories are, in general, partially ergodic. Namely there are regions of initial conditions that generate trajectories with the same long time pattern of points [48]. But only rarely we find globally ergodic systems, where almost all trajectories form the same pattern. In general, the domains of partial ergodicity are separated and there are ordered trajectories besides the chaotic trajectories.

In particular, we found in our work with qubits [48] that Born’s distribution itself consists, in general, of both chaotic and ordered trajectories. In exceptional cases, it contains only ordered or only chaotic trajectories. If Born’s distribution contains ordered trajectories and we start with a set of initial conditions different from that of Born’s rule, then we will never reach it unless we have the correct proportion (and distribution) of the ordered trajectories. The case of qubits is excellent for our studies, since the positions of the infinitely many nodal points could be found analytically. Moreover, their positions in the configuration space have a characteristic geometry.

The question now is what the proportion of ordered trajectories in systems with many nodal points scattered in an arbitrary way in the configuration space (namely without a special geometry of their positions) is. This is not an easy problem to deal with. The larger the number of nodes, the higher the complexity of the Bohmian trajectories, something that implies very difficult numerical integrations. These integrations become even more difficult when we also have to integrate the variational equations in order to calculate the Lyapunov characteristic number.

In this paper, the characterization of the Bohmian trajectories as ordered or chaotic is made by applying the practical numerical method described in the Appendix A of [34]. Namely, in order to avoid the calculation of the Lyapunov characteristic number of each trajectory, we exploit the ergodicity (global or local) of the chaotic trajectories. We measured the size of the long-time-limit colorplots [48] of the points of many chaotic trajectories (with a sampling step $\Delta t = 0.05$) initiated in various regions of the support of the wavefunction, and compared them with the colorplot of each trajectory in our ensemble. If the colorplots were similar, then the trajectory was characterized as chaotic. Otherwise, it was characterised as ordered. In the present case, we integrated the distributions up to $t = 10^5$, which was sufficiently large for a chaotic trajectory trapped in a certain region of the configuration space to escape and cover a much larger space. This can be seen in Figure 9, where we show two different time instances $t = 10^2$, and $t = 10^5$ of an ordered (red) trajectory and a chaotic (blue) trajectory. They both are produced by the wavefunction $\Psi = a\Psi_{0,2} + b\Psi_{3,4} + c\Psi_{5,7}$. In the ordered trajectory, we observe that the motion is confined in a area and very quickly acquires its final shape (Figure 9a,b). On the other hand, the chaotic trajectory resembles an ordered trajectory at $t = 10^3$ (Figure 9c) since it has a distorted Lissajous shape in a confined region of space, but later it has many close encounters with the unstable points of the Bohmian flow and covers a large part of the support of Ψ in a complex way (Figure 9d). Thus, it is chaotic.

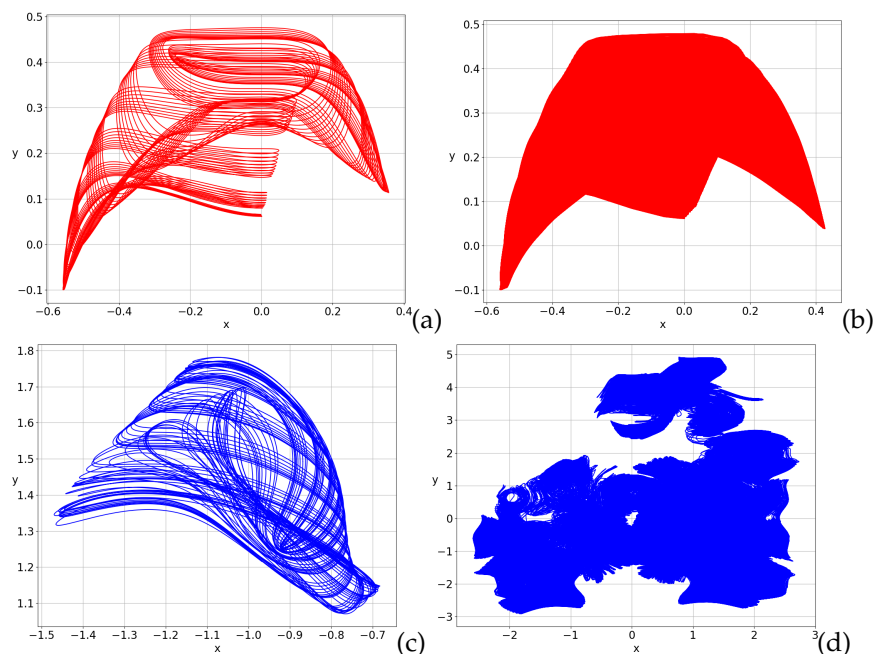


Figure 9. An ordered trajectory (red) and a chaotic Bohmian trajectory of the wavefunction $\Psi = a\Psi_{0,2} + b\Psi_{3,4} + c\Psi_{5,7}$ with $a = 1, b = \sqrt{2}, c = \sqrt{2}/2, \omega_x = 1, \omega_y = \sqrt{2}/2$ for $t \in [0, 10^2]$ (a,c) and for $t \in [0, 10^5]$ (b,d). The ordered trajectory preserves its shape and size over time, while the blue trajectory acquires a very complex shape in space due to its many close encounters with the X and Y unstable points (note that the scale of (d) is much larger than that of (c)).

In Figure 10, we present our results in three different Born distributions made out of 5000 Bohmian particles. In the left panel, we present the initial conditions on the x-y

plane, while in the right panel, we project them onto the surface of $P_0 = |\Psi_0|^2$. The red color corresponds to initial conditions that were found to produce ordered trajectories and the blue color to chaotic trajectories correspondingly. In Figure 10a,b, we have the Born distribution of the wavefunction $\Psi = a\Psi_{0,2} + b\Psi_{3,4} + c\Psi_{5,6}$. A first look at P_0 is enough to understand the complexity of this multinodal wavefunction by taking into consideration that P evolves in a complex way. However, we find that the ordered trajectories in this case form almost 72% of the total set, while the chaotic trajectories are only 28%. This surprising result shows this is the way the the nodes evolve over time, and not just the number of nodes required for chaos to occur [31]. In this case, the collisions between the ‘blobs’ of P are such that most trajectories remain in regions of high P and do not encounter the moving nodal points at the lower levels of P . In fact, as we have already pointed out, in the case of entangled qubits [48], where we have well-defined blobs of P , their collisions are more efficient in producing chaotic trajectories than when the blobs are significantly deformed during the collisions.

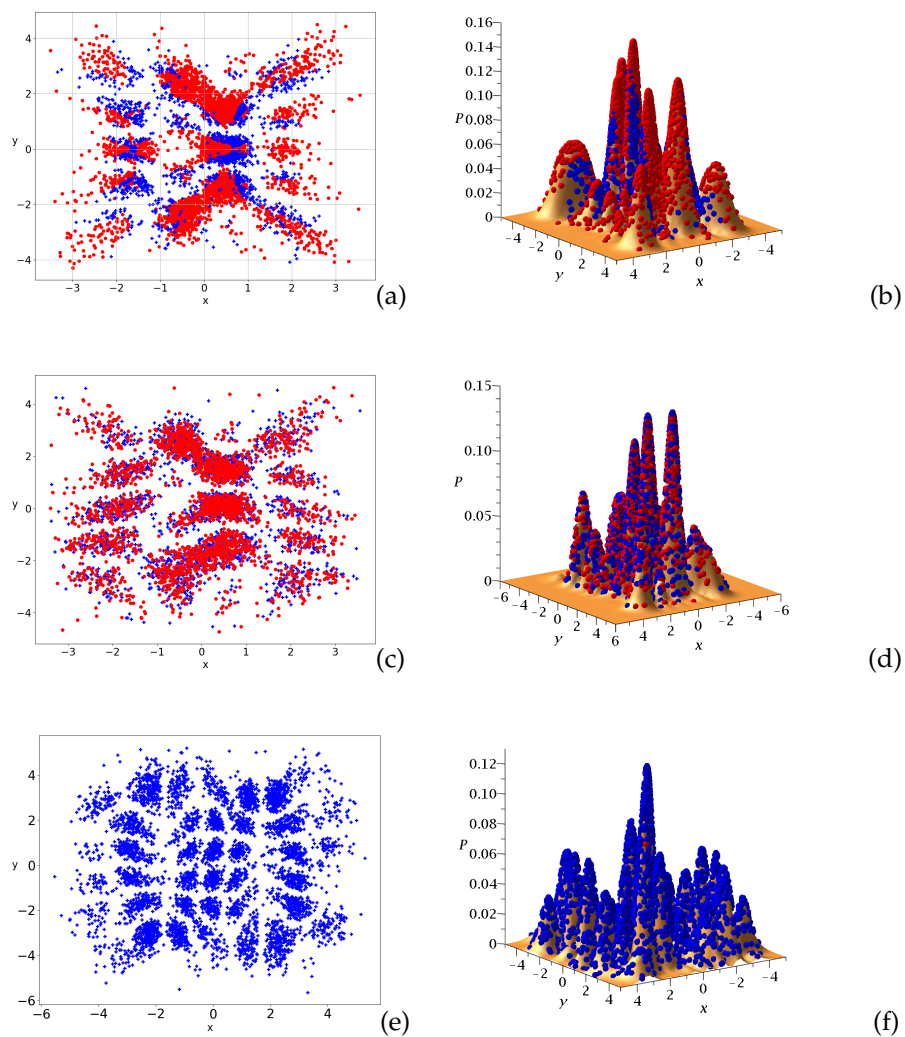


Figure 10. (a) Born’s rule distribution of 5000 particles and its projection on the probability density P_0 in the case of (a,b) $\Psi = a\Psi_{0,2} + b\Psi_{3,4} + c\Psi_{5,6}$. (c,d) $\Psi = a\Psi_{0,2} + b\Psi_{3,4} + c\Psi_{5,7}$ and (e,f) $\Psi = a\Psi_{10,3} + b\Psi_{4,5} + c\Psi_{7,8}$. Red/blue color refers to the initial conditions that produce ordered/chaotic trajectories. The proportion of the ordered trajectories in the first case is 72%, in the second case is 50.6%, and in the third case is practically 0 (in all cases $a = 1, b = \sqrt{2}, c = \sqrt{2}/2, \omega_x = 1, \omega_y = \sqrt{2}/2$).

In Figure 10c,d, we have the wavefunction $\Psi = a\Psi_{0,2} + b\Psi_{3,4} + c\Psi_{5,7}$. By changing only the last quantum number, we find a significant increase in chaotic trajectories, which are now practically equal to the ordered ones (50,6% and 49,4% correspondingly). Namely,

a slight variation in the system resulted in a drastic change in the amount of its ordered and chaotic trajectories. The collisions between the blobs of P now become more efficient.

However, if one significantly changes the number of the nodes, then it is reasonable to expect chaos to dominate in the Born distribution. This is shown in Figure 10c,d, where we study the wavefunction $\Psi = a\Psi_{10,3} + b\Psi_{4,5} + c\Psi_{7,8}$. There, we find only one ordered trajectory in our sample. Chaos is absolutely dominant in this case.

6. Conclusions

In the present paper, we presented the most important cases in the dynamics of Bohmian systems systems described by superpositions of 2, 3 or multiple energy eigenstates of the 2D quantum harmonic oscillator $V = \frac{1}{2}(M_x\omega_x^2x^2 + M_y\omega_y^2y^2)$.

These systems have, in general, a number of moving nodal points, where $\Psi = 0$. Close to a nodal point (x_N, y_N) , there is an unstable point X in the frame of reference of the nodal point $(u = x - x_N, v = y - y_n)$. Further unstable points (Y-points) appear in the inertial frame of reference (x, y) . Trajectories that approach the X-points or the Y-points are deviated along the unstable asymptotic curves of these points and become chaotic.

However, there are cases where no chaos appears at all, as in the superpositions of two components with constant weight coefficients and phases. There, we showed that the nodal points are stationary, and thus, the X-points coincide with the Y-points. No trajectory can come arbitrarily close to the Y-points, regardless of the number of nodal points. We then showed, by use of stroboscopic sections, how the gradual introduction of an imaginary part in the coefficients of the superposition is able to lead to the emergence of chaos.

In the cases of three (or more) components, there are, in general, both chaotic and ordered trajectories. However, we found that there are special cases of wavefunctions with large quantum numbers but with no chaos.

Then, we considered cases of two qubits of the form (38) made of coherent states of the oscillator. In these systems, there are infinitely many energies in the Poisson distribution. This fact implies the existence of infinitely many nodes. However, in practice, one has to make a truncation at some order. The truncated wavefunctions can be written as a superpositions of the energy eigenstates of the quantum harmonic oscillator (with the proper coefficients) and lead to a number of nodal points in space with a complex geometry. There, we showed the gradual change in the position of the nodal points, as we increase the truncation order, and their limiting geometry in the full qubit case where they lie along a straight line.

We note that quantum entanglement is a prerequisite for a Bohmian system to exhibit chaotic behaviour. The absence of entanglement in the wavefunction implies decoupled Bohmian equations, and consequently, ordered Bohmian trajectories. However, entanglement, although necessary, does not always imply chaos, e.g., in the case of commensurable frequencies, we find only ordered trajectories.

In our previous works, with qubit systems (see, e.g., [48,50,56]), we calculated the entanglement by using the von Neumann entropy and we found that it plays a major role in the production of chaotic Bohmian trajectories.

If a distribution of particles initially satisfies Born's rule, then it satisfies it for all times. If the trajectories are only chaotic-ergodic, then any initial distribution will reach Born's rule in the long run. However, the Born distribution consists, in general, of both ordered and chaotic trajectories. Thus, an arbitrary initial distribution does not reach the Born distribution, unless it has the correct proportion and distribution of the ordered trajectories.

In this paper, we explicitly showed that the common belief that a high number of nodal points always leads to the dominance of chaos (and partial or complete ergodicity) is not always correct. We studied the Born distributions of several multinodal wavefunctions and presented a case where order is dominant, a case where chaos is dominant, and a case where order and chaos are almost equal.

The coexistence of order and chaos in the Born distributions is of fundamental importance, not only from the standpoint of the dynamical approach of Born's rule, but also

for understanding how Bohmian trajectories produce the same experimental results as standard quantum mechanics. The details, however, are not yet well understood. Thus, the role of order and chaos in producing the average values of the quantum observables in the above cases is an important open problem for a future study.

Author Contributions: Conceptualization, A.C.T. and G.C.; methodology, A.C.T.; formal analysis, G.C.; investigation, A.C.T.; writing—original draft, G.C.; visualization, A.C.T.; supervision, G.C. All authors have read and agreed to the published version of the manuscript.

Funding: This research received no external funding.

Data Availability Statement: The datasets generated during the current study are available from the corresponding author upon reasonable request.

Acknowledgments: This research was conducted in the framework of the program of the RCAAM of the Academy of Athens “Study of the dynamical evolution of the entanglement and coherence in quantum systems”.

Conflicts of Interest: The authors declare no conflict of interest.

Appendix A

A simple truncated case of the entangled qubits is when $n_f = 1$. Then, Equations (36) and (37) take the form

$$Y = e^{-\frac{a_0^2}{2}} e^{-\frac{i}{2}\omega_q t} \left(\frac{1}{\sqrt[4]{\pi}} \sqrt[4]{\omega_q} e^{-\frac{\omega_q q^2}{2}} + \frac{a_0 e^{i\sigma_q} e^{-i\omega_q t} \sqrt{2} q}{\sqrt[4]{\pi}} \omega_q^{\frac{3}{4}} e^{-\frac{\omega_q q^2}{2}} \right), \quad q = x, y. \quad (A1)$$

The phases $\sigma_q = 0$ and $\sigma_q = \pi$ correspond to $Y = Y_R$ and $Y = Y_L$. Thus, the wavefunction of the system is

$$\Psi = \frac{(\omega_x \omega_y)^{\frac{1}{4}}}{\sqrt{\pi}} e^{-a_0^2 - \frac{\omega_x x^2}{2} - \frac{\omega_y y^2}{2}} \left((c_1 + c_2) e^{-\frac{i}{2}t(\omega_x + \omega_y)} + \sqrt{2} \sqrt{\omega_x} a_0 x (c_1 - c_2) e^{-\frac{i}{2}t(\omega_y + 3\omega_x)} - \sqrt{2} \sqrt{\omega_y} a_0 y (c_1 - c_2) e^{-\frac{i}{2}t(3\omega_y + \omega_x)} - 2(c_1 + c_2) \sqrt{\omega_x} \sqrt{\omega_y} e^{-3/2it(\omega_x + \omega_y)} a_0^2 xy \right). \quad (A2)$$

In the large parenthesis, there are four terms—a constant with respect to x, y , two linear terms in x or y , and a quadratic cross term with xy . Therefore, the wavefunction contains terms of the form $\Psi_{0,0}, \Psi_{0,1}, \Psi_{1,0}$ and $\Psi_{1,1}$. In this case, we find that for nonzero and not equal c_1, c_2 , there are two nodal points. In fact, if we eliminate the cross term by appropriate multiplications in Ψ_R, Ψ_L , then we find an equation with linear terms in x and y . Thus, y is a linear function of x , and if we insert this function into Ψ , we find a quadratic equation for x .

For $c_1 c_2 = 0$, we have a decoupled system with no isolated nodal points, while for $c_1 = c_2$ (and $n_f = 1$), there is no fixed nodal point and the Bohmian flow is periodic in time. In the last case, all the trajectories are periodic following the arguments of Section 2. Thus, in order to observe chaos in the maximally entangled case $c_1 = c_2 = \sqrt{2}/2$, we need $n_f \geq 2$.

References

- de Broglie, L. Interference and corpuscular light. *Nature* **1926**, *118*, 441. [CrossRef]
- de Broglie, L. La mécanique ondulatoire et la structure atomique de la matière et du rayonnement. *J. Phys. Radium* **1927**, *8*, 225. [CrossRef]
- Bohm, D. A Suggested Interpretation of the Quantum Theory in Terms of “Hidden” Variables. I. *Phys. Rev.* **1952**, *85*, 166. [CrossRef]
- Bohm, D. A Suggested Interpretation of the Quantum Theory in Terms of “Hidden” Variables. II. *Phys. Rev.* **1952**, *85*, 180. [CrossRef]
- Holland, P.R. *The Quantum Theory of Motion: An Account of the de Broglie-Bohm Causal Interpretation of Quantum Mechanics*; Cambridge University Press: Cambridge, UK, 1995.

6. Sanz, A. Bohm's approach to quantum mechanics: Alternative theory or practical picture? *Front. Phys.* **2019**, *14*, 11301. [[CrossRef](#)]
7. Benseny, A.; Albareda, G.; Sanz, Á.S.; Mompart, J.; Oriols, X. Applied Bohmian mechanics. *Eur. Phys. J. D* **2014**, *68*, 286. [[CrossRef](#)]
8. Madelung, E. Quantum theory in hydrodynamical form. *Z. Phys.* **1927**, *40*, 322. [[CrossRef](#)]
9. Chiarelli, P.; Chiarelli, S. Stability of Quantum Eigenstates and Collapse of Superposition of States in a Fluctuating Vacuum: The Madelung Hydrodynamic Approach. *Eur. J. Appl. Phys.* **2021**, *3*, 11–28. [[CrossRef](#)]
10. Beyer, M.; Paul, W. On the Stochastic Mechanics Foundation of Quantum Mechanics. *Universe* **2021**, *7*, 166. [[CrossRef](#)]
11. Philippidis, C.; Dewdney, C.; Hiley, B.J. Quantum interference and the quantum potential. *Nuovo Cimento B (1971–1996)* **1979**, *52*, 15. [[CrossRef](#)]
12. Goldstein, S.; Struyve, W. On quantum potential dynamics. *J. Phys. A* **2014**, *48*, 025303. [[CrossRef](#)]
13. Tzemos, A.; Contopoulos, G. Bohmian quantum potential and chaos. *Chaos Sol. Fract.* **2022**, *160*, 112151. [[CrossRef](#)]
14. Wimberger, S. *Nonlinear Dynamics and Quantum Chaos*; Springer: Berlin/Heidelberg, Germany, 2014.
15. Robnik, M. Fundamental concepts of quantum chaos. *Eur. Phys. J. Spec. Top.* **2016**, *225*, 959. [[CrossRef](#)]
16. Contopoulos, G. *Order and Chaos in Dynamical Astronomy*; Springer: Berlin/Heidelberg, Germany, 2002.
17. Wiggins, S. *Introduction to Applied Nonlinear Dynamical Systems and Chaos*; Springer: Berlin/Heidelberg, Germany, 2003.
18. Parmenter, R.H.; Valentine, R. Deterministic chaos and the causal interpretation of quantum mechanics. *Phys. Lett. A* **1995**, *201*, 319. [[CrossRef](#)]
19. Sengupta, S.; Chattaraj, P. The quantum theory of motion and signatures of chaos in the quantum behaviour of a classically chaotic system. *Phys. Lett. A* **1996**, *215*, 119. [[CrossRef](#)]
20. Iacomelli, G.; Pettini, M. Regular and chaotic quantum motions. *Phys. Lett. A* **1996**, *212*, 29. [[CrossRef](#)]
21. Frisk, H. Properties of the trajectories in Bohmian mechanics. *Phys. Lett. A* **1997**, *227*, 139. [[CrossRef](#)]
22. Wu, H.; Sprung, D. Quantum chaos in terms of Bohm trajectories. *Phys. Lett. A* **1999**, *261*, 150. [[CrossRef](#)]
23. Cushing, J.T. Bohmian insights into quantum chaos. *Philos. Sci.* **2000**, *67*, S430. [[CrossRef](#)]
24. Makowski, A.; Pełowski, P.; Dembiński, S. Chaotic causal trajectories: the role of the phase of stationary states. *Phys. Lett. A* **2000**, *266*, 241. [[CrossRef](#)]
25. Makowski, A.J.; Frackowiak, M. The simplest non-trivial model of chaotic causal dynamics. *Acta Phys. Pol. B* **2001**, *32*, 2831.
26. Makowski, A.J. Forced Dynamical Systems Derivable from Bohmian Mechanics. *Acta Phys. Pol. B* **2002**, *33*, 583.
27. Falsaperla, P.; Fonte, G. On the motion of a single particle near a nodal line in the de Broglie–Bohm interpretation of quantum mechanics. *Phys. Lett. A* **2003**, *316*, 382. [[CrossRef](#)]
28. Wisniacki, D.A.; Pujals, E.R. Motion of vortices implies chaos in Bohmian mechanics. *Europhys. Lett.* **2005**, *71*, 159. [[CrossRef](#)]
29. Wisniacki, D.; Pujals, E.; Borondo, F. Vortex dynamics and their interactions in quantum trajectories. *J. Phys. A* **2007**, *40*, 14353. [[CrossRef](#)]
30. Borondo, F.; Luque, A.; Villanueva, J.; Wisniacki, D.A. A dynamical systems approach to Bohmian trajectories in a 2D harmonic oscillator. *J. Phys. A* **2009**, *42*, 495103. [[CrossRef](#)]
31. Cesa, A.; Martin, J.; Struyve, W. Chaotic Bohmian trajectories for stationary states. *J. Phys. A* **2016**, *49*, 395301. [[CrossRef](#)]
32. Contopoulos, G.; Tzemos, A.C. Chaos in Bohmian quantum mechanics: A short review. *Regul. Chaotic Dyn.* **2020**, *25*, 476. [[CrossRef](#)]
33. Tzemos, A.C.; Contopoulos, G. Bohmian chaos in multinodal bound states. *Found. Phys.* **2022**, *52*, 85. [[CrossRef](#)]
34. Tzemos, A.C.; Contopoulos, G. Unstable Points, Ergodicity and Born's Rule in 2D Bohmian Systems. *Entropy* **2023**, *25*, 1089. [[CrossRef](#)] [[PubMed](#)]
35. Efthymiopoulos, C.; Kalopotharakos, C.; Contopoulos, G. Origin of chaos near critical points of quantum flow. *Phys. Rev. E* **2009**, *79*, 036203. [[CrossRef](#)] [[PubMed](#)]
36. Ballentine, L.E. *Quantum Mechanics: A Modern Development*; World Scientific: Singapore, 2014.
37. Valentini, A. Signal-locality, uncertainty, and the subquantum H-theorem. I. *Phys. Lett. A* **1991**, *156*, 5–11. [[CrossRef](#)]
38. Valentini, A. Signal-locality, uncertainty, and the subquantum H-theorem. II. *Phys. Lett. A* **1991**, *158*, 1–8. [[CrossRef](#)]
39. Dürr, D.; Goldstein, S.; Zanghi, N. Quantum chaos, classical randomness, and Bohmian mechanics. *J. Stat. Phys.* **1992**, *68*, 259. [[CrossRef](#)]
40. Valentini, A.; Westman, H. Dynamical origin of quantum probabilities. *Proc. R. Soc. A Math. Phys. Eng. Sci.* **2005**, *461*, 253. [[CrossRef](#)]
41. Towler, M.; Russell, N.; Valentini, A. Time scales for dynamical relaxation to the Born rule. *Proc. R. Soc. A Math. Phys. Eng. Sci.* **2011**, *468*, 990. [[CrossRef](#)]
42. Norsen, T. On the explanation of Born-rule statistics in the de Broglie-Bohm pilot-wave theory. *Entropy* **2018**, *20*, 422. [[CrossRef](#)] [[PubMed](#)]
43. Dürr, D.; Struyve, W., Typicality in the foundations of statistical physics and Born's rule. In *Do Wave Functions Jump? Perspectives of the Work of GianCarlo Ghirardi*; Springer: Berlin/Heidelberg, Germany, 2021; p. 35.
44. Lustosa, F.B.; Pinto-Neto, N.; Valentini, A. Evolution of quantum non-equilibrium for coupled harmonic oscillators. *Proc. R. Soc. A* **2023**, *479*, 20220411. [[CrossRef](#)]
45. Valentini, A. Astrophysical and cosmological tests of quantum theory. *J. Phys. A* **2007**, *40*, 3285. [[CrossRef](#)]
46. Valentini, A. Inflationary cosmology as a probe of primordial quantum mechanics. *Phys. Rev. D* **2010**, *82*, 063513. [[CrossRef](#)]

47. Colin, S.; Valentini, A. Mechanism for the suppression of quantum noise at large scales on expanding space. *Phys. Rev. D* **2013**, *88*, 103515. [[CrossRef](#)]
48. Tzemos, A.; Contopoulos, G. The role of chaotic and ordered trajectories in establishing Born's rule. *Phys. Scr.* **2021**, *96*, 065209. [[CrossRef](#)]
49. Horodecki, R.; Horodecki, P.; Horodecki, M.; Horodecki, K. Quantum entanglement. *Rev. Mod. Phys.* **2009**, *81*, 865. [[CrossRef](#)]
50. Tzemos, A.C.; Contopoulos, G. Ergodicity and Born's rule in an entangled three-qubit Bohmian system. *Phys. Rev. E* **2021**, *104*, 054211. [[CrossRef](#)] [[PubMed](#)]
51. Zander, C.; Plastino, A. Revisiting Entanglement within the Bohmian Approach to Quantum Mechanics. *Entropy* **2018**, *20*, 473. [[CrossRef](#)] [[PubMed](#)]
52. Elsayed, T.A.; Mølmer, K.; Madsen, L.B. Entangled Quantum Dynamics of Many-Body Systems using Bohmian Trajectories. *Sci. Rep.* **2018**, *8*, 12704. [[CrossRef](#)] [[PubMed](#)]
53. Sanz, A. Young's experiment with entangled bipartite systems: The role of underlying quantum velocity fields. *Entropy* **2023**, *25*, 1077. [[CrossRef](#)]
54. Garrison, J.; Chiao, R. *Quantum Optics*; Oxford Univ. Press: Oxford, UK, 2008.
55. Nielsen, M.A.; Chuang, I.L. *Quantum Computation and Quantum Information*; Cambridge University Press: Cambridge, UK, 2004.
56. Tzemos, A.C.; Contopoulos, G.; Efthymiopoulos, C. Bohmian trajectories in an entangled two-qubit system. *Phys. Scr.* **2019**, *94*, 105218. [[CrossRef](#)]

Disclaimer/Publisher's Note: The statements, opinions and data contained in all publications are solely those of the individual author(s) and contributor(s) and not of MDPI and/or the editor(s). MDPI and/or the editor(s) disclaim responsibility for any injury to people or property resulting from any ideas, methods, instructions or products referred to in the content.